Electronic Structure, Defect Chemistry, and Transport Properties of $SrTi_{1-x}Fe_xO_{3-y}$ Solid Solutions

Avner Rothschild,*,† Wolfgang Menesklou,‡ Harry L. Tuller,† and Ellen Ivers-Tiffée‡

Department of Materials Science and Engineering, Massachusetts Institute of Technology, 77 Massachusetts Avenue, Cambridge, Massachusetts 02139, and Institut für Werkstoffe der Elektrotechnik, Universität Karlsruhe (TH), 76131 Karlsruhe, Germany

Received December 19, 2005. Revised Manuscript Received May 10, 2006

The electronic structure, defect chemistry, and transport properties of members of the mixed ionic electronic conducting $SrTi_{1-x}Fe_xO_{3-y}$ (STF) solid-solution system are revisited, and an improved defect chemical model is proposed in which Fe is considered to be one of the main constituents that shape the energy-band structure of STF, rather than an impurity dopant with acceptor-like character. As a consequence of the high inherent deficiency in the oxygen sublattice, introduced by the mixed-valence states of the B-site cations Ti^{4+} and Fe^{3+}, oxygen vacancies and interstitials generated by the anion Frenkel reaction dominate the defect equilibria, leading to predominant ionic conductivity at intermediate partial pressures of oxygen. Increasing Fe content results in both a systematic decrease in band-gap energy, $E_g^0 = 3.2 - 1.9x + 0.5x^2$ eV, and reduction enthalpy, $\Delta H_{red} = 5.8 - 3.4x + 1.7x^2$ eV. The decrease in band gap is explained on the basis of the systematic broadening of the Fe-derived 3d band lying above the O-derived 2p valence band. The Fe-induced changes in band structure were experimentally confirmed by both optical and photoelectron (XPS) spectroscopies.

Introduction

Mixed ionic electronic conductors (MIEC or mixed conductors for short) with high electronic and oxygen-ion conductivities play an important role in solid-state electrochemical devices designed for energy conversion and gas sensing. Important applications include solid oxide fuel cell (SOFC) electrodes, oxygen separation membranes, insertion electrodes, electrochromic windows, oxygen sensors, gas sensors, and catalysts.[1−3] As demonstrated in the following, the $SrTi_{1-x}Fe_xO_{3-y}$ family (STF for short), which forms a continuous solid solution between strontium titanate ($SrTiO_3$) and strontium ferrite ($SrFeO_3$) over the entire composition range $0 < x < 1$,[4] serves as a model MIEC system. Whereas strontium titanate is a wide-band-gap semiconductor ($E_g^0 = 3.2$ eV at $T = 0$ K)[5] with rather low conductivity levels in the pristine (undoped) state,[6] strontium ferrite is a mixed conductor with high levels of electronic and ionic conductivities, on the order of ∼100 and ∼0.2 S/cm, respectively, at high temperature (850 °C).[7] Strontium ferrite, however, undergoes an order−disorder transition at $T = 830$ °C from a disordered perovskite phase ($SrFeO_3$, space group $Pm\bar{3}m$) to an ordered brownmillerite phase ($Sr_2Fe_2O_5$, space group *Icmm*),[8,9] rendering it incompatible for many important applications. Nevertheless, it has been found that substitution of Ti for Fe stabilizes the perovskite phase[4] while retaining high levels of ionic and electronic conductivities, especially for Fe-rich compositions ($x > 0.1$).[10,11] This makes the STF family an important MIEC system with prospective applications in oxygen permeation membranes,[11] solid oxide fuel cells,[12] oxygen sensors,[13] and hydrocarbon gas sensors.[14]

Indeed, a number of research groups have investigated the STF system using X-ray,[4,10,15] neutron,[17,18] and electron diffraction[10,15] techniques to determine the crystal structure, Mössbauer spectroscopy and magnetic susceptibility measurements to examine the valence state and coordination of Fe,[16−18] and electron energy loss spectroscopy (EELS) to probe the electronic structure.[10] These studies confirmed the existence of a continuous solid-solution system with a pseudo-perovskitic structure in the entire composition range $0 < x < 1$. Unlike the end member strontium ferrite, no

* Corresponding author. E-mail: avner@mit.edu.
† Massachusetts Institute of Technology.
‡ Universität Karlsruhe (TH).

(1) Tuller, H. L. *Solid State Ionics* **1997**, *94*, 63.
(2) Boivin, J. C.; Mairesse, G. *Chem. Mater.* **1998**, *10*, 2870.
(3) Skinner, S. J.; Kilner, J. A. *Mater. Today* **2003**, *3*, 30.
(4) Brixner, L. H. *Mater. Res. Bull.* **1968**, *3*, 299.
(5) Choi, G. M.; Tuller, H. L.; Goldschmidt, D. *Phys. Rev. B* **1986**, *34*, 6972.
(6) Choi, G. M.; Tuller, H. L. *J. Am. Ceram. Soc.* **1988**, *71*, 201.
(7) Patrakeev, M. V.; Leonidov, I. A.; Kozhevnikov, V. L.; Kharton, V. V. *Solid State Sci.* **2004**, *6*, 907.
(8) Takeda, Y.; Kanno, K.; Takada, T.; Yamamoto, O.; Takano, M.; Nakayama, N.; Bando, Y. *J. Solid State Chem.* **1986**, *63*, 237.
(9) Mizusaki, J.; Okayasu, M.; Yamauchi, S.; Fueki, K. *J. Solid State Chem.* **1992**, *99*, 166.
(10) Steinsvik, S.; Bugge, R.; Gjønnes, J.; Taftø, J.; Norby, T. *J. Phys. Chem. Solids* **1997**, *58*, 969.
(11) Jurado, J. R.; Figueiredo, F. M.; Gharbage, B.; Frade, J. R. *Solid State Ionics* **1999**, *118*, 89.
(12) Fagg, D. P.; Kharton, V. V.; Kovalevsky, A. V.; Viskup, A. P.; Naumovich, E. N.; Frade, J. R. *J. Eur. Ceram. Soc.* **2001**, *21*, 1831.
(13) Menesklou, W.; Schreiner, H. J.; Härdtl, K. H.; Ivers-Tiffée, E. *Sens. Actuators, B* **1999**, *59*, 184.
(14) Sahner, K.; Moos, R.; Matam, M.; Tunney, J. J.; Post, M. *Sens. Actuators, B* **2005**, *108*, 202.
(15) Greaves, C.; Buker, R. A. *Mater. Res. Bull.* **1986**, *21*, 823.
(16) Rodriguez, J.; Pereda, J. A.; Vallet, M.; Calbet, J. G.; Tejada, J. *Mater. Res. Bull.* **1986**, *21*, 255.
(17) Gibb, T. C.; Battle, P. D.; Bollen, S. K.; Whitehead, R. J. *J. Mater. Chem.* **1992**, *2*, 111.
(18) Adler, P.; Eriksson, S. *Z. Anorg. Allg. Chem.* **2000**, *626*, 118.

10.1021/cm052803x CCC: $33.50
Published on Web 07/14/2006

evidence for long-range ordering of oxygen vacancies in STF has been presented. It is noteworthy, however, that evidence for short-range ordering of oxygen vacancies about random Fe sites is reported in this system.[10,15,16,18] In addition to these studies, the transport properties of STF were investigated quite extensively using electrical conductivity measurements as function of oxygen partial pressure and temperature,[10] electrochemical permeability measurements,[11] impedance spectroscopy,[19] thermogravimetric (TG) measurements, and coulometric titration.[20] Despite all of these studies, the electronic structure and defect chemistry of STF, and their effect on the transport properties, remain poorly understood.[11,20]

The shortcoming of the previous investigations to provide a self-consistent picture that effectively correlates crystal structure, electronic structure, defect chemistry, and transport properties largely lies in underestimating the role of Fe in the system. Previous studies often relied on the dilute solution Fe-doped $SrTiO_3$ model system, whose electronic structure, defect chemistry, and transport properties are well-known,[5,6,21−24] and simply extended the model to include Fe concentrations that cover the entire composition range ($0 < x < 1$). We note, that although possible modifications in the equilibrium constants (e.g., the band-gap energy) for different STF compositions were taken into account in some of these studies,[10,11,13,19,20] Fe was still regarded as an impurity with an acceptor-like character similar to its role in $SrTiO_3$. However, the extension of the Fe-doped $SrTiO_3$ model to high Fe concentrations (> ca. 1 mol %) is inappropriate, because it does not satisfy the conditions of the dilute solution defect model and disregards the extended nature of the electronic states derived from Fe at such high concentrations, where these states overlap with one another and form admixtures with the O 2p valence states.[25,26] This simplified model also fails to predict the increase in both the electron and hole conductivities with increasing Fe concentration, as shown in Figure 1.[27] In contrast, on the basis of conventional point defect thermodynamics, the concentration of electrons (and *n*-type conductivity) should decrease with increasing acceptor concentrations,[28] as was shown by Chan et al. for the case of Al-doped $BaTiO_3$ with small Al concentrations (<0.15 mol %).[29] Furthermore, it was reported that this model failed to account for thermogravimetric and coulometric titration measurements of intermediate STF compositions.[20]

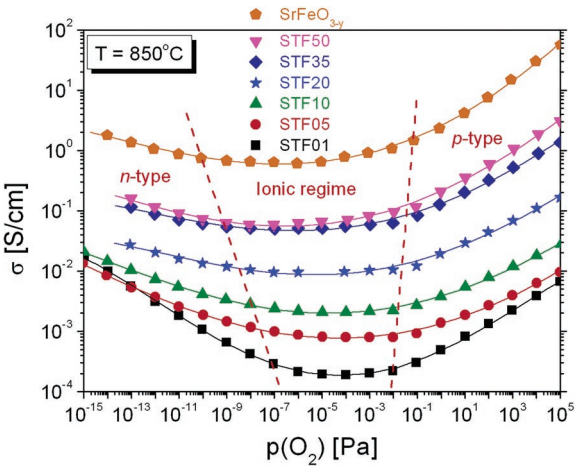

Figure 1. Electrical conductivity (σ) isotherms, at $T = 850$ °C, as a function of oxygen partial pressure ($p(O_2)$) for different STF compositions with Fe concentrations between 1 mol % (STF01) and 50 mol % (STF50), as well as $SrFeO_{3-y}$.[31]

In this contribution, we revisit the electronic structure and defect chemistry of STF and propose a self-consistent approach for describing the correlations between these features and the transport properties of STF. In view of the abovementioned observations, Fe is considered to be one of the main constituents that shape the energy-band structure of STF, similar to Ti, Sr, and O, rather than an impurity dopant with acceptor-like character. Thus, STF is treated here as a solid-solution system between the end members strontium titanate and strontium ferrite. This implies that the properties of intermediate STF compositions systematically evolve from the characteristic properties of the two end members. Although this work specifically considers the STF system, the underlying approach is applicable to other solid solution systems and therefore may shed new light on the defect chemistry and the resulting electronic and ionic transport properties of other MIEC.

Experimental Section

STF powders with different Fe/Ti ratios were prepared by the conventional mixed-oxide technique, starting from commercial $SrCO_3$ (Merck, Selectipur, 99%), TiO_2 (Bayer, Bayertitan PK5594, 99.7%), and Fe_2O_3 (Merck p.A., 99%) powders. The powders were mixed in appropriate amounts to obtain the desired Fe/Ti ratios, ball milled for 2 h, and subsequently calcined in air at 1200 °C for 15 h. Phase and chemical compositions were examined by X-ray diffraction (XRD, Siemens D5000) and X-ray energy dispersion spectroscopy (EDS, Oxford INCA 200 Analyzer). These examinations confirmed that under the temperature ($700 < T < 1000$ °C) and oxygen partial pressure ($1 \times 10^{-13} < p(O_2) < 1 \times 10^5$ Pa) conditions reported in this work, the STF powders had a single-phase perovskite structure.[30]

Thermogravimetric (TG) measurements were carried out at temperatures between 800 and 1000 °C in air, 10 mol % O_2/N_2, 5 mol % O_2/N_2, and pure N_2 (with a residual O_2 concentration of

(19) Jurado, J. R.; Colomer, M. T.; Frade, J. R. *Solid State Ionics* **2001**, *143*, 251.
(20) Ferreira, A. A. L.; Abrantes, J. C. C.; Jurado, J. R.; Frade, J. R. *Solid State Ionics* **2000**, *135*, 761.
(21) Chan, N.-H.; Sharma, R. K.; Smyth, D. M. *J. Electrochem. Soc.* **1981**, *128*, 1762.
(22) Denk, I.; Münch, W.; Maier, J. *J. Am. Ceram. Soc.* **1995**, *78*, 3265.
(23) Moos, R.; Härdtl, K. H. *J. Am. Ceram. Soc.* **1997**, *80*, 2549.
(24) Akhtar, M. J.; Akhtar, Z.-U.-N.; Jackson, R. A.; Catlow, C. R. A. *J. Am. Ceram. Soc.* **1995**, *78*, 421.
(25) Evarestov, R. A.; Piskunov, S.; Kotomin, E. A.; Borstel, G. *Phys. Rev. B* **2003**, *67*, 64101.
(26) Zhou, H. D.; Goodenough, J. B. *J. Solid State Chem.* **2004**, *177*, 1952.
(27) It is noted that a similar observation was also made in ref 10, but no explanation was given for the discrepancy between the model predictions and the empirical results.
(28) Smyth, D. M. *The Defect Chemistry of Metal Oxides*; Oxford University Press: Oxford, 2000.
(29) Chan, N. H.; Sharma, R. K., Smyth, D. M. *J. Am. Ceram. Soc.* **1982**, *65*, 167.
(30) Schneider, T. Strontiumtitanferrit−Abgassensoren, Stabilitätsgrenzen/Betriebsfelder (Strontium−Titanate−Ferrite-Based Exhaust Gas Sensors, Stability Limits/Characteristic Diagrams). Ph.D. Thesis (in German), Universität Karlsruhe (TH). Karlsruhe, Germany, 2005; Verlag−Mainz: Aachen, Germany, 2006.

~10 ppm) gas mixtures. A symmetric thermobalance (Model TG439, Netzsch, Selb, Germany), designed with two gas-tight ovens, compares the oxygen partial pressure dependent weight of the STF powder samples (≈27.6 mg) to the oxygen partial pressure independent weight of a reference (sapphire, 27.6 mg). Because of this symmetric measuring system, gas buoyancy effects are very small (<0.01 μg) and can be neglected for the specified temperature range and gas flow (100 mL/min).

For electrical testing, polycrystalline ceramic pellets (5 × 5 × 15 mm^3) were cold-pressed and sintered in air at 1400 °C for 10 h. Their density, estimated by the He gas pycnometer method (Micromeritics Accupyc 1300), was 95% of the theoretical value, and an average grain size of 5 μm was determined by SEM. The pellets were sliced (between 0.3 and 1 mm long) and contacted with four Pt wires using Pt paste (Demetron 308 A). Four-point probe conductivity measurements (DC) were carried out using a conventional current and voltage measurement setup (Keithley Instruments). The equilibrium values of the electrical conductivity were measured in a tube furnace equipped with an oxygen pump capable of adjusting the oxygen pressure between 1×10^{-13} and 1×10^{5} Pa in the temperature range 700−1000 °C. It is noted that these measurements were carried out by Heilig,[31] and some of them were published in a previous paper.[13] In this contribution, we re-evaluate the experimental results as part of our defect chemical model. For more details on the preparation method of the STF pellets and the electrical measurements as functions of oxygen partial pressure and temperature, the reader is referred to the respective references.[13,31] We further note that in addition to the DC measurements, AC impedance spectroscopy measurements were also carried out to deconvolute between possible contributions to the overall (DC) resistance from the grains, grain boundaries, and other macroscopic features, as often observed in polycrystalline ceramics.[32] However, unlike the case of acceptor-doped $SrTiO_3$,[33] we observed single arcs in the complex impedance spectra (Cole−Cole plots), indicating that there were no significant contributions other than the bulk (grain) resistivity. A similar observation was reported by Jurado et al. for intermediate STF compositions.[19] The diameter of those arcs closely matched the DC resistance values, thus confirming the suitability of the DC measurements in providing all the essential information on the electrical behavior of our specimens.

In addition to the ceramic pellets, thin film (~150 nm) specimens of STF35 ($x = 0.35$) and $SrTiO_3$ (for comparison) were also prepared for X-ray photoelectron spectroscopy (XPS), light transmission spectroscopy, and spectroscopic ellipsometry measurements. The films were deposited on (100) oriented MgO substrates (10 × 10 × 0.5 mm^3, MTI Corporation, Richmond, CA) by means of pulsed laser deposition (PLD) from ceramic targets of the respective materials. The substrates were heated to 725 °C during deposition, and the oxygen pressure during deposition was 13.3 Pa. The resulting films had a polycrystalline perovskite structure (determined by XRD) with a typical grain size between 100 and 200 nm (determined by AFM). They were transparent with a dark yellow hue and were optically smooth (surface roughness of ~2 nm, determined by AFM), which is a prerequisite for the respective measurements. The preparation and microstructural characterizations

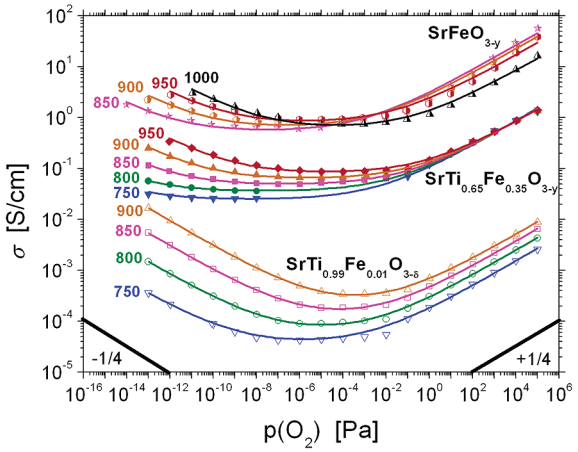

Figure 2. Conductivity isotherms at different temperatures (750−1000 °C) as a function of oxygen partial pressure ($p(O_2)$) for STF compositions with 1 mol % (STF01), 35 mol % (STF35), and 100 mol % Fe ($SrFeO_{3-y}$). Experimental data points[31] are represented by symbols, fitted curves by solid lines.

of these films were described elsewhere.[34] Prior to the measurements, all films were annealed for 10 h at 700 °C in atmospheric air pressure.

XPS spectra were acquired using a Kratos AXIS ultra imaging X-ray photoelectron spectrometer equipped with a monochromatized Al Kα small-spot source ($h\nu = 1486.6$ eV) and a 160 mm concentric hemispherical energy analyzer. Light transmission spectra were acquired in the spectral range 190−860 nm using a Perkin−Elmer Lambda 19 UV−vis spectrometer. Variable-angle spectroscopic ellipsometry measurements were carried out in the spectral range 250−2000 nm using a SOPRA GES5 UV−vis−IR high-precision rotating polarizer ellipsometer equipped with a photomultiplier detector for the UV−visible spectrum from 230 to 880 nm and an InGaAs detector in the near infrared spectrum from 880 to 2050 nm. The incident angles were 61, 63, and 65°. These angles were found to give the largest contrast in the ellipsometric parameters for our films. The ellipsometric parameters were fitted using the Levenberg−Marquardt regression method, and the dispersion relations of the refractive indexes were calculated using the standard dielectric function model in the analysis and simulation software WinElli.

Results and Discussion

Electronic Structure. Figure 2 shows the conductivity (σ) data of STF compositions with $x = 0.01$, 0.35, and 1.0 as a function of the partial pressure of oxygen ($p(O_2)$) at different temperatures between 750 and 1000 °C. The results for another composition with $x = 0.5$ are not shown but are also included in the analysis. In this $p(O_2)$ range, i.e., between 1×10^{-13} and 1×10^{5} Pa, the σ vs $p(O_2)$ curves show no evidence of a phase transition and exhibit the bathtub shape that is typically assigned to predominant *n*-type electronic conductivity at low oxygen pressures, ionic conductivity at intermediate oxygen pressures, and *p*-type electronic conductivity at high oxygen pressures.[35] The −1/4 and +1/4 slopes for the electronic components of the conductivity in the *n*- and *p*-type regimes, respectively, indicate that the oxygen vacancy concentration is independent of the partial

(31) Heilig, C. Characterisierung der elekrischen Eigenschaften von Sr(Ti,Fe)O_3 im Hinblick auf die Anwendung in Sauerstoffsensoren (Characterization of the Electrical Properties of Sr(Ti, Fe)O_3 in View of an Application as Oxygen Sensors). Diploma Thesis (in German), Universität Karlsruhe (TH), Karlsruhe, Germany, 1996.
(32) Barsoukov, E.; Macdonald, J. R. *Impedance Spectroscopy: Theory, Experiments, and Applications*, 2nd ed.; Wiley: Hoboken, NJ, 2005.
(33) Waser, R.; Hagenbeck, R. *Acta Mater.* **2000**, *48*, 797.
(34) Litzelman, S. J.; Rothschild, A.; Tuller, H. L. *Sens. Actuators, B* **2005**, *108*, 231.
(35) Spears, M. A.; Tuller, H. L. *Mater. Res. Soc. Proc.* **1995**, *369*, 271.

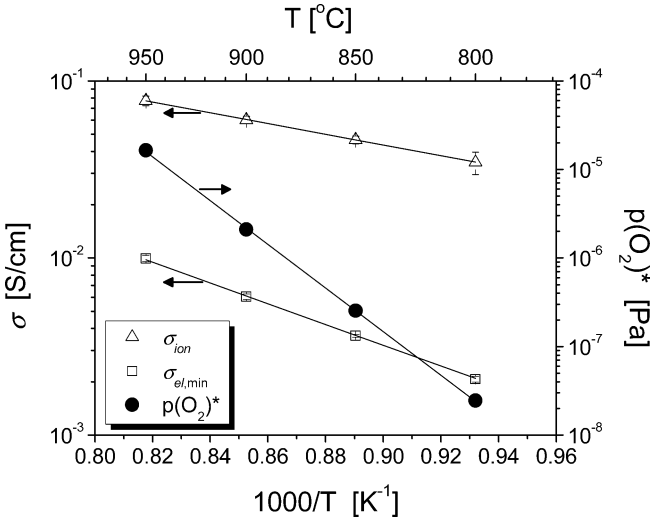

Figure 3. Semilogarithmic Arrhenius plot of σ_{ion}, $\sigma_{el,min}$, and $p(O_2)^*$ vs $1/T$ for STF35.

Table 1. Ionic Conductivity Activation Energies (E_{ion}), Band-Gap Energies (E_g^0), and Redox Enthalpies (ΔH_{red}) for Different STF Compositions

	E_{ion} (eV)	E_g^0 (eV)	ΔH_{red} (eV)
$SrTi_{0.99}Fe_{0.01}O_{3-y}$	1.31 ± 0.06	3.2 ± 0.1	5.8 ± 0.1
$SrTi_{0.65}Fe_{0.35}O_{3-y}$	0.72 ± 0.02	2.7 ± 0.1	4.8 ± 0.1
$SrTi_{0.5}Fe_{0.5}O_{3-y}$	0.66 ± 0.01	2.4 ± 0.1	4.5 ± 0.1
$SrFeO_{3-y}$	0.55 ± 0.02	1.9 ± 0.1	4.1 ± 0.1

pressure of oxygen, and therefore the experimental data were fitted to the following formula used by Yoo et al.[36] to analyze the defect chemistry of $BaTiO_3$, which exhibits a similar behavior:

$$\sigma = \sigma_{el,min} \times \cosh\left[\frac{1}{4}\ln\left(\frac{p(O_2)}{p(O_2)^*}\right)\right] + \sigma_{ion} \qquad (1)$$

Here, $\sigma_{el,min} = 2q(\mu_n\mu_p)^{1/2}n_i$, q is the electronic charge, μ_n and μ_p are the electron and hole mobilities, respectively, n_i is the intrinsic electron (or hole) concentration, σ_{ion} is the ionic conductivity, $p(O_2)^* = (\mu_n/\mu_p)^2 p(O_2)^0$, and $p(O_2)^0$ is the partial pressure of oxygen at the intrinsic point, i.e., when $n = p = n_i$. The fitted curves are shown as solid lines in Figure 2, and one can see that the correlation between the experimental data points and the fitted curves is excellent.

The three fitting parameters σ_{ion}, $\sigma_{el,min}$, and $p(O_2)^*$ were calculated for each data set by using the weighted least-squares regression method in the curve fitting toolbox in MATLAB (version 6.5, MathWorks, 2002). The temperature dependencies of these parameters were subsequently analyzed, as demonstrated in Figure 3 for the case of STF35, to obtain the ionic conductivity activation energy (E_{ion}), band-gap energy at absolute zero (E_g^0), and redox enthalpy (ΔH_{red}) of the respective compositions. The resulting values are given in Table 1. It is noted that our results are in excellent agreement with the band-gap energy and redox enthalpy values reported for the two end members strontium titanate (3.17 and 6.1 ± 0.2 eV, respectively)[23] and strontium ferrite (2 and 4 eV, respectively).[37]

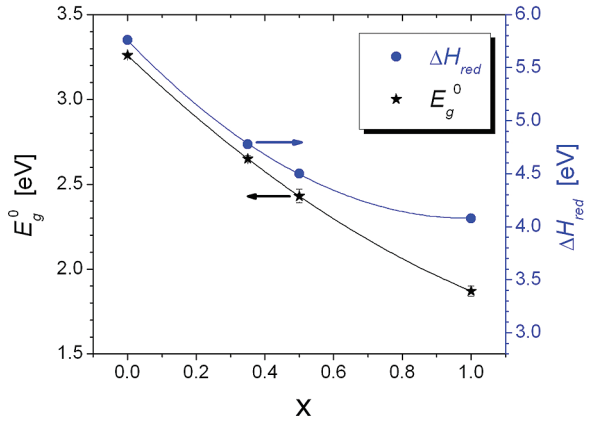

Figure 4. Band-gap energy and redox enthalpy as a function of Fe content (x) in $SrTi_{1-x}Fe_xO_{3-y}$ solid solutions.

The variations in band-gap energy and redox enthalpy as a function of composition (x) are shown in Figure 4. One can see that they both vary systematically between the characteristic values of the two end members strontium titanate and strontium ferrite. Furthermore, the variations in band-gap energy and redox enthalpy follow parabolic laws, $E_g^0 = 3.2 - 1.9x + 0.5x^2$ eV and $\Delta H_{red} = 5.8 - 3.4x + 1.7x^2$ eV. Interestingly enough, a similar behavior is well-known for the band-gap energy of III−V semiconductor alloys such as $Ga_xIn_{1-x}P$ and $GaAs_xSb_{1-x}$, wherein the parabolic term (i.e., the bowing parameter) arises from the increasing disorder due to alloying.[38] Thus, unlike previous studies that regarded Fe in STF solid solutions as an impurity dopant with acceptor-like character,[10,11,13,19,20] we argue that it should instead be considered as being one of the main constituents that sets the atomic potential field that the electronic carriers experience as they travel through the crystal and therefore participates in shaping the band structure of STF, just like the other constituents Sr, Ti, and O. In other words, in contrast to the Fe-doped $SrTiO_3$ system with low Fe concentrations (<1 mol %), Fe can no longer be considered as being a defect in STF.

To confirm the observation of decreasing band-gap energy with increasing Fe concentration, complementary optical and XPS measurements were carried out using STF35 and $SrTiO_3$ films deposited by PLD on MgO substrates. Figure 5 shows the transmission spectra of both films in the UV−visible range (190−860 nm). Interference patterns (fringes), often observed in such transparent thin film structures,[39] make it difficult to determine the fundamental absorption edge corresponding to the onset of the band-to-band transition. To circumvent these difficulties, we carried out spectroscopic ellipsometry measurements in the spectral range 250−2000 nm. The ellipsometric parameters were fitted using the Levenberg−Marquardt regression method, and the dispersion relations of the refractive indexes were calculated using the standard dielectric function model in the analysis and simulation software WinElli (SOPRA-SA, France). This model combines the Cauchy law, Drude model, and standard critical point model to calculate the dispersion relations in the UV term, IR term, and special peaks in the spectra,

(36) Yoo, H. I.; Song, C. R.; Lee, D. K. *J. Electroceram.* **2002**, *8*, 5.
(37) Kozhevnikov, V. L.; Leonidov, I. A.; Patrakeev, M. V.; Mitberg, E. B.; Poeppelmeier, K. R. *J. Solid State Chem.* **2000**, *158*, 320.
(38) Van Vechten, J. A.; Bergstresser, T. K. *Phys. Rev. B* **1970**, *1*, 3351.
(39) Swanepoel, R. *J. Phys. E: Sci. Instrum.* **1983**, *16*, 1214.

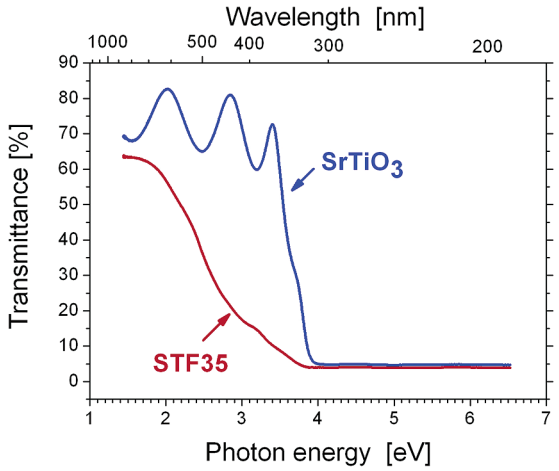

Figure 5. Optical transmission spectra of STF35 and $SrTiO_3$ thin films (~150 nm) on MgO substrates.

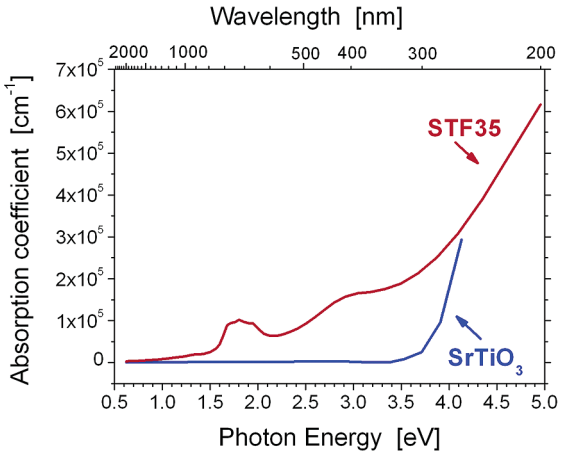

Figure 6. Optical absorption spectra calculated from spectroscopic ellipsometry measurements of STF35 and $SrTiO_3$ thin films (~150 nm) on MgO substrates.

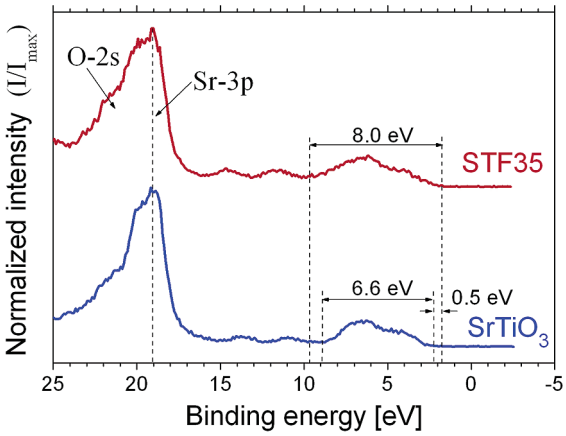

Figure 7. Photoelectron spectra of STF35 and $SrTiO_3$ thin films (~150 nm) on MgO substrates.

respectively. The resulting absorption spectra are shown in Figure 6. One can see that the absorption edge of STF35 indeed occurs at considerably lower photon energy than for $SrTiO_3$, in agreement with our model. The most conclusive observation in support of our model is given in Figure 7, wherein the XPS spectra, in the range of low binding energies (<25 eV), shows that the valence band of STF35 is broader than that for $SrTiO_3$ by ~1.4 eV and extends closer to the conduction band edge by approximately 0.5 eV, which

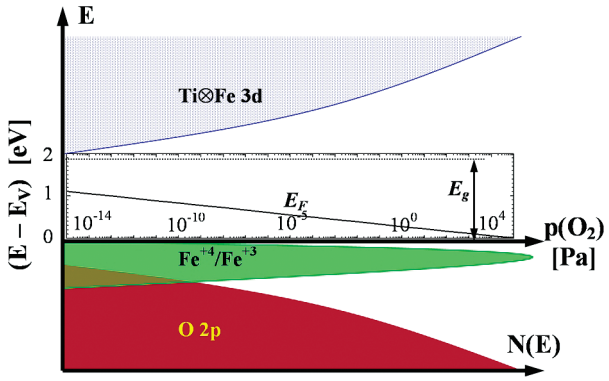

Figure 8. Schematic energy-band diagram of STF50. The variation in the Fermi level (E_F) as function of the partial pressure of oxygen is on the basis of calculations for STF50 at $T = 850$ °C.

corresponds to the reduction in the band-gap energy of these compositions according to our results (see Table 1).

In view of these results, Figure 8 depicts the proposed band structure of STF. The band-gap energy (E_g) and the position of the Fermi level (E_F), the latter as a function of the partial pressure of oxygen ($p(O_2)$), are calculated for STF50 at $T = 850$ °C on the basis of results obtained from our defect chemical model (see below). We propose that the top of the valence band consists largely of Fe 3d and O 2p states that readily form covalent admixtures because the Fe^{4+}/Fe^{3+} redox state lies near the top of the O 2p band.[26] A similar situation has been reported for strontium ferrite.[40] The bottom of the conduction band is assigned to Ti 3d states that, given the proximity of the Fe^{3+}/Fe^{2+} redox state to the conduction band edge of $SrTiO_3$,[41] are expected to form admixtures with Fe 3d states. In view of the energetics and the character of the respective states, we expect the degree of overlap between the Fe- and O-derived states at the top of the valence band to be smaller than for the Fe and Ti conduction band states. Consequently, holes are expected to have a higher tendency toward localization by potential fluctuations at the top of the valence band rather than the electrons, which experience a smoother interatomic potential field.[42] We further note that the width of the Fe-derived band is expected to increase with increasing Fe concentrations given the enhanced overlap of the respective electronic states with one another or with the O 2p states.[42] Indeed, this effect has been reported recently by Evarestov et al., who calculated the bandwidth of the impurity band introduced by substitution of Fe for Ti in $SrTiO_3$ to increase from 0.14 to 1.42 eV when the average Fe−Fe distance was reduced from 13.53 to 7.81 Å, corresponding to Fe concentrations of 2.4 to 12.5 mol %, respectively.[25] Thus, with increasing Fe concentrations, the valence band edge is expect to shift closer to the conduction band, consistent with our observation of systematically decreasing band-gap energies as a function of Fe concentration (see Table 1 and Figure 4).

(40) Bocquet, A. E.; Fujimori, A.; Mizokawa, T.; Saitoh, T.; Hamatame, H.; Suga, S.; Kimizuka, N.; Takeda, Y.; Takano, M. *Phys. Rev. B* **1992**, *45*, 1561.
(41) Michel-Calendini, F. M.; Müller, K. A. *Solid State Commun.* **1981**, *40*, 255.
(42) Mott, N. F.; Davis, E. A. *Electronic Processes in Noncrystalline Materials*, 2nd ed.; Clarendon Press: Oxford, U.K., 1979.

Defect Chemistry. Given that the STF system represents a broad solid-solution system, a key salient question is what crystal structure and stoichiometry should be taken as the reference when defining defects in this system. Obvious candidates are the end members, $SrTiO_3$ and $SrFeO_3$, with the cubic perovskite structure ($Pm\bar{3}m$). Although these indeed make logical choices for dilute solutions of Fe-doped $SrTiO_3$ or Ti-doped $SrFeO_3$, respectively, they become less appealing when it comes to intermediate compositions, say for example, $SrTi_{0.5}Fe_{0.5}O_{3-y}$, where both end members contribute equally. Instead, when dealing with concentrated solid solutions, it is much more reasonable to select a lattice framework that accommodates both Fe and Ti in the unperturbed (perfect) state, where neither Fe nor Ti is considered a defect. An obvious complication in selecting that appropriate reference oxygen stoichiometry arises from the different valences of Fe and Ti, which favor, under a wide range of conditions, the +3 and +4 oxidation states, respectively.[4,15,17,18,26] With a divalent cation (Sr^{2+}) on the A site, trivalent cations (Fe^{3+}) on the B site of the perovskite structure (which ideally accommodates only tetravalent cations such as Ti^{4+} in perfectly stoichiometric ABO_3 compositions) must lead to oxygen vacancies in a ratio of one vacancy per two trivalent cations. Given these circumstances and following Brixner,[4] we argue that $SrTi^{+4}_{1-x}Fe^{+3}_{x}O_{3-x/2}$ is a more suitable framework to describe the defect structure of STF rather than $SrTi^{+4}_{1-x}Fe^{+4}_{x}O_3$. The former formulation reflects the tendency of Fe to favor the +3 oxidation state over the +4 state under the experimental conditions in the present study.[43]

The choice of the $SrTi_{1-x}Fe_xO_{3-x/2}$ framework implies partial occupancy of the oxygen sublattice in the perfect (stoichiometric) lattice, with the fraction $x/6$ of the oxygen sites in the archetype ABO_3 perovskitic structure unoccupied. These sites should not be viewed as point defects but rather as an integral part of the perfect lattice (i.e., the framework), and therefore no net charge should be assigned to them. In contrast, if one chooses the $SrTi_{1-x}Fe_xO_3$ lattice as the framework, then the oxygen vacancies introduced by the Fe^{3+} states must also be taken into account. These vacancies would be viewed as defects in the $SrTi_{1-x}Fe_xO_3$ framework, carrying an effective positive charge of 2 which, using the Kröger−Vink notation,[44] are denoted by $V_O^{\bullet\bullet}$. Under these circumstances, Fe^{3+} is considered a defect, in conflict with our notion that Fe must be regarded as one of the main constituents of the structure that, for example, shapes the energy band structure of STF. We further note that the mixed-valence states of Fe are viewed in the $SrTi_{1-x}Fe_xO_{3-x/2}$ framework as filled and empty valence band states, i.e., Fe^{3+} is considered a nondefect (perfect state) and Fe^{4+} a hole, in accord with Figure 8.

Having selected $SrTi_{1-x}Fe_xO_{3-x/2}$ as the appropriate framework, the next question is how does one treat defects in a partially filled oxygen sublattice wherein a significant fraction ($x/6$) of the oxygen sites are unoccupied in the perfect lattice. This issue was examined in detail by Norby and coworkers with regards to the defect chemistry of strontium ferrites and other inherently oxygen deficient systems (i.e., grossly nonstoichiometric oxides).[45−47] They proposed three alternative approaches to describe the intrinsic ionic disorder in such systems. The first approach, the so-called "fully acceptor-doped approach", corresponds to the case of x% Fe-substituted $SrTiO_3$ with $0 < x < 100\%$. We already ruled out this notation on the grounds of the similar role of Fe and Ti in shaping the energy band structure and other physicochemical properties of intermediate STF compositions. The other two alternatives are the "anion Frenkel approach" and the "partial occupancy disordered system approach". The underlying difference between them is that in the former approach, the occupied and unoccupied sites in the oxygen sublattice of the framework structure are inequivalent, whereas in the latter approach, they are equivalent.[45−47]

On the basis of the possible nearest neighbor configurations in the system, there are different types of coordinations around the oxygen sites in STF: all iron (Fe−O−Fe), all titanium (Ti−O−Ti), and mixed iron and titanium (Fe−O−Ti) coordinations. Furthermore, it has been shown recently that iron in strontium ferrite exists in 4-, 5-, and 6-fold coordinations and that the defect energies of oxygen vacancies are different for the corresponding configurations.[48] Given that not all the oxygen sites are equivalent, the anion Frenkel approach is more sensible then the partial occupancy disordered system approach for describing intrinsic ionic disorder in STF. We further note that our neutron powder diffraction and Mössbauer spectroscopy measurements indicate that Fe, in intermediate STF compositions, is largely 5-fold coordinated, whereas Ti is largely 6-fold coordinated.[43] In other words, the unoccupied oxygen sites favor Fe rather then Ti in their nearest-neighbor coordination. This serves as another indication that not all the oxygen sites are equivalent and therefore one can assign normally occupied and unoccupied sites in the ground state of the system. Consequently, anion Frenkel disorder is the most sensible approach in describing intrinsic disorder in the oxygen sublattice of STF despite the fact that, unlike the ordered brownmillerite phases of $Sr_2Fe_2O_5$ and $Ba_2In_2O_5$, whose defect structures have often been modeled using the anion Frenkel disorder,[51,52] long-range ordering has not been observed in STF.[4,15,17] We further note that anion Frenkel disorder, which with increasing temperature increasingly populates unoccupied oxygen sites at the expense of occupied sites in the ground state of the system, represents the transition from a quasi-ordered structure at low temperatures to the disordered structure at high temperatures, similar to the brownmillerite to perovskite transition in $SrFeO_{3-y}$ and $BaInO_{3-y}$. The fact that, unlike these materials, highly

(43) Rothschild, A.; Lufaso, M. W.; Störmer, H.; Becker, K. D.; Menesklou, W.; Ivers-Tiffée, E.; Tuller, H. L. In preparation.
(44) Kröger, F. A. *The Chemistry of Imperfect Crystals*; North-Holland: Amsterdam, 1974; Vol. 1−3.
(45) Bredesen, R.; Norby, T. *Solid State Ionics* **2000**, *129*, 285.
(46) Bredesen, R.; Norby, T.; Bardel, A.; Lynum, V. *Solid State Ionics* **2000**, *135*, 687.
(47) Norby, T. *J. Mater. Chem.* **2001**, *11*, 11.
(48) Bakken, E.; Allan, N. L.; Barron, H. K.; Mohn, C. E.; Todorov, I. T.; Stølen, S. *Phys. Chem. Chem. Phys.* **2003**, *5*, 2237.
(49) Smyth, D. M. *Annu. Rev. Mater. Sci.* **1985**, *15*, 329.
(50) Zhang, G. B.; Smyth, D. M. *Solid State Ionics* **1995**, *82*, 161.
(51) Fisher, C. A. J.; Islam, M. S. *J. Mater. Chem.* **2005**, *15*, 3200.
(52) Fisher, C. A. J.; Islam, M. S. *Solid State Ionics* **1999**, *118*, 355.

ordered structures have not been observed in the STF system probably relates to the fact that long-range ordering of Fe and Ti is, apparently, difficult to achieve.

In addition to oxygen vacancies ($V_O^{\bullet\bullet}$) and interstitials (O_i''), introduced by the anion Frenkel disorder, the defect model of STF should also take into account cation vacancies (e.g., V_{Sr}'') and unintentional background impurities. However, given the small diffusivities of cation defects with respect to anion defects in perovskite-related oxides, the concentrations of all cation defects are expected to be fixed (frozen-in) below about 1000 °C, whereas the oxygen vacancy and interstitial concentrations continue to equilibrate with the ambient conditions (temperature and oxygen pressure) down to about 500 °C, below which the kinetics become too slow.[23,53] Because our measurements were carried out between 750 and 1000 °C, the ionic defects considered in our defect chemical model include oxygen vacancies and interstitials, whose concentrations are actively controlled by equilibrium defect processes (see below) and a constant concentration of defects that accounts for all the frozen-in cation defects, $C = \sum z_i C_i =$ constant, where z_i and C_i denote the charge and concentration of the ith defect. The sign convention we use is that z_i is positive for positively charged defects (e.g., $z = 1$ for $La_{Sr}^{\bullet}$) and negative for negatively charged defects (e.g., $z = -2$ for V_{Sr}''). We also assume that the majority of the ionic defects are fully ionized in the relevant temperature range where our model is valid (~500 °C < T < ~1000 °C). With these assumptions, the electroneutrality condition becomes

$$n + 2[O_i''] = p + 2[V_O^{\bullet\bullet}] + C \tag{2}$$

The dominant defect reactions are (1) electron−hole generation via thermal ionization across the band gap (intrinsic electronic disorder); (2) thermal generation of oxygen vacancies and interstitials via the anion Frenkel reaction (intrinsic ionic disorder); and (3) equilibration of the oxygen activity in the solid and gas phases that leads to oxygen deficiency ($\delta < 0$) or excess ($\delta > 0$) in the inherently oxygen deficient $SrTi_{1-x}Fe_xO_{3-(x/2)+\delta}$ lattice under reducing ($p(O_2) < p(O_2)^0$) or oxidizing ($p(O_2) > p(O_2)^0$) conditions, respectively. Note that the latter reaction (see eq 5 below) is just an alternative formulation of the redox reaction.[54] The corresponding mass action laws are[28]

$$np = n_i^2 = K_I = N_C N_V \exp(-E_g/kT) \tag{3}$$

$$[V_O^{\bullet\bullet}][O_i''] = K_{AF} = [O_O^x][V_i^x] \exp(\Delta S_{AF}/k) \exp(-\Delta H_{AF}/kT) \tag{4}$$

$$\frac{[V_O^{\bullet\bullet}]}{[V_O^{\bullet\bullet}]_0}\left(\frac{n}{n_i}\right)^2\left(\frac{p(O_2)}{p(O_2)^0}\right)^{1/2} = 1 \tag{5}$$

where $N_{C,V} = 4.82 \times 10^{15}(m_{e,h}^*/m_0)^{3/2}T^{3/2}$ cm^{-3} are the effective densities of states at the bottom of the conduction band and top of valence band. $m_{e,h}^*$ are the effective masses of electrons and holes, m_0 is the free electron mass, $[O_O^x] = (3 - (1/2)x)$[STF] and $[V_i^x] = (1/2)x$[STF] are the concentrations of oxygen lattice and interstitial sites, respectively, [STF] $= 1/V_{unit\_cell}$ is the number of STF molecular formula units per unit volume, and $[V_O^{\bullet\bullet}]_0$ is the oxygen vacancy concentration at the stoichiometric oxygen pressure, i.e., when $p(O_2) = p(O_2)^0$. ΔS_I and ΔS_{AF} are the entropies associated with reactions 3 and 4, respectively. We note that the band-gap energy (E_g) decreases with increasing temperatures following a linear relationship, $E_g(T) = E_g^0 - aT$, where E_g^0 is the band-gap energy at absolute zero ($T = 0$ K) and α is typically on the order of 1×10^{-4} to 1×10^{-3} eV/K ($\alpha = 5.7 \times 10^{-4}$ eV/K for $SrTiO_3$).[23]

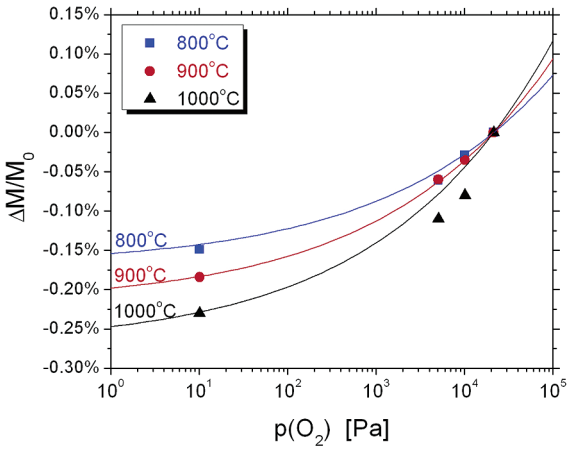

Figure 9. Thermogravimetric data of mass change (ΔM) with respect to the specimen mass in air (M_0) for STF35 at different oxygen partial pressures and temperatures. Experimental data points are represented by symbols, fitted curves by solid lines. The apparent deviation between the fitted curve and the experimental data points at $T = 1000$ °C could arise from experimental errors due to thermal drift of the TG apparatus.

The equilibrium constants K_I and K_{AF} and $p(O_2)^0$ were obtained by fitting the conductivity and TG data as a function of oxygen partial pressure and temperature, as shown in Figures 2 and 9, respectively. The results are summarized in Table 2. Using these values, the defect concentrations can be calculated as functions of T and $p(O_2)$ for different STF compositions by solving eqs 2−5, as shown exemplarily in Figure 10 for the case of STF50 at $T = 900$ °C. We note that, except for STF01 (1 mol % Fe), the concentrations C of fixed cation defects were found to be much smaller than the concentrations of oxygen vacancies and interstitials. In fact, a reliable evaluation of C could not be obtained for the other STF compositions due to the dominancy of $[V_O^{\bullet\bullet}]$ and $[O_i'']$.

The electron (σ_n) and hole conductivities (σ_p) were found to have a power-law dependence on the oxygen partial pressure, $\sigma_n \propto p(O_2)^{-1/4}$ and $\sigma_p \propto p(O_2)^{1/4}$, respectively. These dependencies are expected for n and p, respectively, from the redox reaction and electron−hole reaction (eqs 5 and 3) under conditions where the activity of the oxygen vacancies is independent of $p(O_2)$. This condition holds true for STF given the fact that the concentrations of oxygen vacancies and interstitials are largely fixed by the extensive intrinsic disorder in the oxygen sublattice wherein the redox reaction has only minor effect on these values, as demonstrated in Figure 10. Finding the same $p(O_2)$ dependencies for the partial electronic conductivities as those predicted for the corresponding electronic carrier densities confirms that the

(53) Tsur, Y.; Dunbar, T. D.; Randall, C. A. *J. Electroceram.* **2001**, *7*, 25.
(54) Tsur, Y.; Randall, C. A. *J. Am. Ceram. Soc.* **2001**, *9*, 2147.

Table 2. Key Defect Reactions and Equilibrium Constants for $SrTi_{1-x}Fe_xO_{3-y}$ Solid Solutions

defect reaction	mass action law	equilibrium constants
$e_{vb} + h_{cb} \leftrightarrow e_{cb}' + h_{vb}^{\bullet}$	$np = K_I = N_C N_V \exp(-E_g/kT)$ $N_{C,V} = 4.82 \times 10^{15}(m^*_{e,h}/m_0)^{3/2}T^{3/2}$ (cm^{-3})	$3 < m^*_{e,h}/m_0 < 12$ $E_g^0 = 3.2 - 1.9x + 0.5x^2$ (eV) $\alpha = 5.7 \times 10^{-4}$ eV/K
$O_O + V_i \leftrightarrow V_O^{\bullet\bullet} + O_i''$	$[V_O^{\bullet\bullet}][O_i''] = K_{AF} = (3 - x/2)(x/2)[STF]^2 \exp(\Delta S_{AF}/k)\exp(-\Delta H_{AF}/kT)$ $[STF] = 1.64 \times 10^{22}$ [cm^{-3}]	$\Delta S_{AF} = 1k$ $\Delta H_{AF} = 0.4 \pm 0.1$ (eV)
$O_O \leftrightarrow V_O^{\bullet\bullet} + 2e_{cb}' + 1/2O_2$	$([V_O^{\bullet\bullet}]/[V_O^{\bullet\bullet}]_0)(n/n_1)^2(p(O_2)/p(O_2)^0)^{1/2} = 1$ $[V_O^{\bullet\bullet}]_0 = (K_{AF})^{1/2}$; $n_i = (K_I)^{1/2}$	$p(O_2)^0 \sim \exp(-\Delta H_{red}/kT)$ $\Delta H_{red} = 5.8 - 3.4x + 1.7x^2$ (eV)

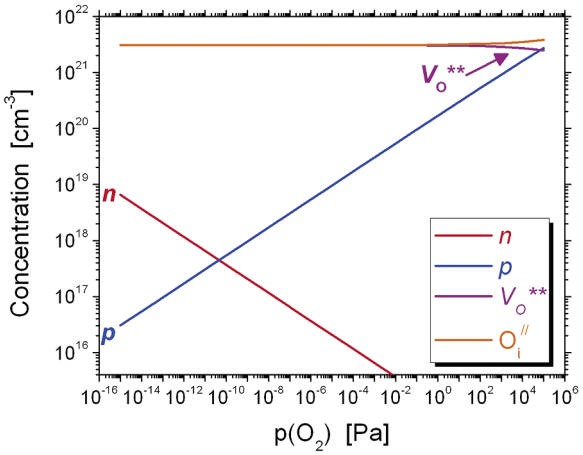

Figure 10. Kröger−Vink diagram of defect concentrations as function of the partial pressure of oxygen in STF50 at $T = 900$ °C. Note the domination of the Frenkel reaction over nearly the full range of the partial pressure of oxygen.

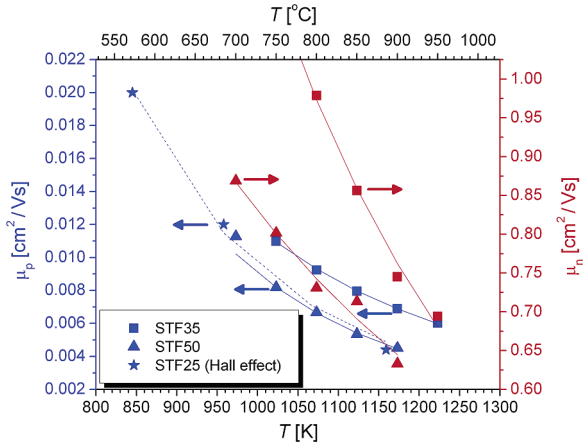

Figure 11. Calculated electron and hole mobilities for STF35 and STF50. The experimental hole mobility values of STF25, obtained by Hall effect measurements,[31] are shown for comparison purposes.

electron and hole mobilities remain independent of $p(O_2)$ under the studied conditions.

Given the relationship between the electron concentration and Fermi level in semiconducting materials, $n = N_C \exp(-E_F/kT)$, one can see that the power-law dependence of n on $p(O_2)$ leads to $E_F \propto -(1/4)kT \ln[p(O_2)]$, where E_F is measured from the valence band edge (i.e., $E_V = 0$). The dependence of the Fermi level on the oxygen partial pressure and temperature can be written as

$$E_F(T,p(O_2)) = \frac{E_g^0 - \alpha T}{2} - \frac{3kT}{4}\ln\left(\frac{m_h^*}{m_e^*}\right) - \frac{kT}{4}\ln\left(\frac{p(O_2)}{p(O_2)^0}\right) \quad (6)$$

This relationship enables one to calculate the Fermi level as function of T and $p(O_2)$ using the defect chemical equilibrium constants (see Table 2). An example of such calculation is depicted in Figure 8 for the case of STF50 at $T = 850$ °C. We note that such representations of isothermal variations in E_F as function of $p(O_2)$ are equivalent to isothermal defect diagrams (i.e. Kröger−Vink diagrams),[28] such as the one shown in Figure 10.

Electronic Transport Properties. By combining the conductivity data in Figure 2 with our defect chemical analysis, we obtained the transport properties of the electronic and ionic carriers in STF as follows. We remind the reader that σ_{ion}, $\sigma_{el,min}$, and $p(O_2)^*$ were calculated by fitting the conductivity data in Figure 2 to eq 1 (see Figure 3). Thus, once the equilibrium constants K_I and $p(O_2)^0$ have been determined in our defect chemical analysis (see Table 2), the electron and hole mobility values (μ_n and μ_p, respectively) are obtained from the relationships $\mu_n\mu_p = (\sigma_{el,min}/2q)^2/K_I$ and $\mu_n/\mu_p = [p(O_2)^*/p(O_2)^0]^{1/2}$.[36] Figure 11 shows the electron and hole mobility values obtained by this method for STF35 and STF50. Note that the resultant hole mobility values for STF35 are in rather good agreement with the experimental Hall effect results for STF25.[31,55]

Both electron and hole mobilities were found to decrease with increasing temperatures following a power-law temperature dependence, $\mu \propto T^{-m}$, as shown in Table 3. This indicates that the transport mechanisms for electrons and holes follow, most likely, the bandlike rather than the small polaron model in the respective temperature range (550−950 °C). In the bandlike model, the mobility decreases with increasing temperatures because of scattering by lattice vibrations (phonons), whose displacements increase with temperature and therefore more strongly scatter electronic carriers. In contrast, the mobility of small polarons increases exponentially with temperature, $\mu \propto \exp(-E_H/kT)$, because of the activated nature of the polaron hopping mechanism (E_H is the hopping energy).[42] Ideally, the power exponent m is calculated to be 3/2 for scattering by acoustic phonons, but in practice, m is typically larger than that because of additional scattering mechanisms such as intervalley or optical phonon scattering, which result in steeper μ vs T dependencies.[56] We note that electron transport in $SrTiO_3$ and $BaTiO_3$ is known to follow the itinerant electron (band) mechanism, which, at high temperatures, is dominated by phonon scattering with $2.7 < m < 3.2$ for $SrTiO_3$ and $m = 2.9$ for $BaTiO_3$.[57,58] These values are in reasonable agreement

(55) Rothschild, A.; Litzelman, S. J.; Tuller, H. L.; Menesklou, W.; Schneider, T.; Ivers-Tiffeé, E. *Sens. Actuators, B* **2005**, *108*, 225.
(56) Lundstrom, M. *Fundamentals of Carrier Transport*, 2nd ed.; Cambridge University Press: Cambridge, U.K., 2000.
(57) Frederikse, H. P. R.; Hosler, W. R. *Phys. Rev. B* **1966**, *144*, 734.
(58) Kolodiazhnyi, T.; Petric, A.; Niewczas, M.; Bridges, C.; Safa-Sefat, A.; Greedan, J. E. *Phys. Rev. B* **2003**, *68*, 85205.

Table 3. Electron and Hole Mobilities of Different STF Compositions

composition	electron mobility (cm^2/Vs)	hole mobility (cm^2/Vs)
STF35	$\mu_n = (1.97 \pm 0.02) \times 10^8 \times T^{(2.7 \pm 0.2)}$	$\mu_p = (1.6 \pm 0.6) \times 10^8 \times T^{(3.4 \pm 0.1)}$
STF50	$\mu_n = (4.71 \pm 0.05) \times 10^4 \times T^{(1.6 \pm 0.3)}$	$\mu_p = (1.7 \pm 0.1) \times 10^{11} \times T^{(4.4 \pm 0.1)}$
STF25[a]		$\mu_p = (2.8 \pm 0.8) \times 10^{11} \times T^{(4.5 \pm 0.5)}$

[a] On the basis of Hall effect measurements in air at 572 °C < T < 886 °C.[31]

with our results (e.g., $m = 2.7$ for STF35), suggesting that electron transport in STF also follows a bandlike mechanism.

Figure 11 shows that the hole mobility of STF is almost 2 orders of magnitude smaller than the electron mobility and has a steeper temperature dependence (see Table 3). In contrast, the hole mobility of Fe-doped $SrTiO_3$ (0.2 mol % Fe) has a temperature dependence similar to that of the electron mobility, with $m = 2.36$.[59] Given the difference between the Fe^{4+}/Fe^{3+} redox state and the top of the valence band in $SrTiO_3$ (~1.1 eV),[41] this discrepancy could be attributed to fluctuations in the interatomic potential field felt by the holes as they travel through the lattice, as mentioned earlier. Such effects can lead to enhancement of the mobility temperature dependence in inhomogeneous semiconductors ($2 < m < 4$)[60] and other disordered systems ($2 < m < 4.5$).[61] We note that at low temperatures, the electronic carriers in such systems tend to be localized because of trapping by local minima (pockets) in the potential field; consequently, the electronic conduction tends to follow a hopping mechanism, but at high temperatures they become delocalized by thermal ionization into the extended states above those traps and therefore the high-temperature conduction mechanism follows a bandlike model.[61] This process is also known as thermal ionization to delocalized states above the mobility gap.[42]

Conclusions

$SrTi_{1-x}Fe_xO_{3-y}$ (STF) solid solutions exhibit mixed ionic electronic conductivity at elevated temperatures, with predominant contributions from electrons (*n*-type conductivity), oxygen vacancies and interstitials (ionic conductivity), and holes (*p*-type conductivity) at low, intermediate, and high partial pressures of oxygen, respectively. All three contributions increase with increasing Fe/Ti ratios, consistent with reduced band-gap energies and reduction enthalpies and increasing levels of disorder in the oxygen sublattice introduced by substitution of Ti^{4+} by Fe^{3+}. The concentrations of these defects are determined by the balance between the intrinsic electronic (band-to-band ionization) and ionic (anion Frenkel) disorder reactions and the redox reaction. The respective equilibrium constants and the defect mobilities were obtained by analyzing conductivity and TG data of different STF compositions as functions of oxygen partial pressure and temperature. It was found that the equilibrium constants, such as those represented by the band-gap energy and reduction enthalpy, vary systematically across the composition range $0 \leq x \leq 1$ between the characteristic values of the two end members strontium titanate ($x = 0$) and strontium ferrite ($x = 1$).

Although this work specifically considers the STF system, the underlying approach is applicable to other solid solution systems and therefore may assist in shedding light on the defect chemistry and the resulting electronic and ionic transport properties of other mixed ionic electronic conductors.

Acknowledgment. This work was supported by the German Ministry of Education and Research (BMBF PTJ-NMT 03N3102). A.R. acknowledges a grant from the Fulbright Foundation for a postdoctoral fellowship. The authors thank Dr. Thomas Schneider for the TG measurements, Dr. Il-Doo Kim for PLD deposition of the $SrTiO_3$ and STF35 thin films, Ms. Elisabeth L. Shaw for the XPS measurements, and Prof. Yoel Fink for permission to use his spectroscopic ellipsometry facilities. This work made use of MRSEC Shared Experimental Facilities at MIT, supported by the National Science Foundation under Award DMR-02-13282.

CM052803X

(59) Fleischer, M.; Meixner, H.; Tragut, C. *J. Am. Ceram. Soc.* **1992**, *75*, 1666.
(60) Karpov, V. G.; Shik, A. Y.; Shklovskii, B. I. *Sov. Phys. Semicond.* **1982**, *16*, 901.
(61) Blaise, G. *J. Electrost.* **2001**, *50*, 69.